

Electrical Properties and Conductivity Mapping of Thin Multilayered Films Containing Different Types of Carbon Nanotubes

Hye Jin Park,^{†,‡} Kyoung Ah Oh,^{‡,§,||} Min Park,[§] and Hyunjung Lee^{*,§}

Hybrid Materials Research Center, Korea Institute of Science and Technology, Seoul 136-791, Korea; and Division of Chemical Engineering, Yonsei University, Seoul 120-749, Korea

Received: February 24, 2009; Revised Manuscript Received: May 26, 2009

This study compared the electrical conductivities of transparent films containing carbon nanotubes with different wall numbers (single-wall nanotubes (SWNTs), thin-wall nanotubes (TWNTs), and multiwall nanotubes (MWNTs)). A layer-by-layer fabrication method was chosen to achieve fine control over film transparency. This produced homogeneously dispersed carbon nanotube–polymer composite films over the whole sample area because the method prevents the self-aggregation of carbon nanotubes. Electrical conductivity measurements using the four-probe method showed that TWNTs formed better electrically conductive films than SWNTs and MWNTs. Conductive atomic force microscopy revealed that the distribution of conductive channels depends on the morphology of the nanotubes with different wall numbers in the composite. The close-packed networks of TWNTs in the composite film provided the most effective conductive channels after thermal annealing at 300 °C.

Introduction

Transparent conductive thin film (TCF) electrodes are widely used in liquid crystal displays,¹ touch screens,² solar cells,^{3–5} and flexible displays.^{6–8} Because of their high electrical conductivity and optical transparency, indium tin oxide (ITO) thin films dominate such applications.⁷ However, the limited available resources and high cost of ITO make it necessary to find substitutes that are mechanically flexible, more cost-effective, and can be rolled into films under more practical conditions.^{9,10} One of the most reliable candidates for TCF electrodes are composites of carbon nanotubes (CNTs) on glass or polymer substrates, which harness the extraordinary electrical, physical, and thermal properties of CNTs.^{11–14} Recently, promising results, very low sheet resistance ($\sim 100 \Omega/\text{sq}$) and high transmittance ($>80\%$ at 550 nm), have been reported for CNT thin films made by depositing CNTs onto polymer films via various deposition techniques such as filtration,^{7,15} spray coating,^{9,16} drop casting from solvents,¹⁷ spin coating,^{13,18} and Langmuir–Blodgett deposition.¹⁹ However, the deposition of CNTs onto polymer films still has disadvantages such as the weak adhesion between the CNT layers and polymer substrate and the relatively rough and porous surface of the final product, which could cause serious problems depending on the application.²⁰ In this regard, CNT–polymer composite films could be a good candidate to counteract those disadvantages.^{20–23} Such a CNT–polymer composite has been shown to have undesirably low electrical conductivity due to encapsulation by the polymer and the inhomogeneous distribution of CNTs within the polymer matrix. In addition, conducting polymers have the potential disadvantage of poor stability; that is, the electrical conductivity of the composite film decreases over time due to the oxidization of the conducting polymer. However, we believe further

development of CNT–polymer composite thin films can create new opportunities for their application to TCF electrodes. In this study, we chose insulating polymers as the matrix of the composite film and fabricated a thin CNT–polymer composite films via layer-by-layer (LBL) assembly to investigate the formation of CNT networks with regard to the nanoscale morphology and changes in electrical properties and transparency of the composite film. LBL assembly is one of the most reliable nanofabrication methods for reaching monomolecular-level homogeneity from virtually any nanoscale building block via the sequential deposition of nanometer-thick layers of polymer and nanocolloids.²⁴ LBL also makes it possible to produce CNT composites with exceptional homogeneity by overcoming the self-aggregation of CNTs.^{25–28}

Since the electronic and optical properties of CNTs vary greatly with their structure,^{29,30} we performed a comparative study on CNTs with different wall numbers in terms of their use in simple transparent conductive composite films.³¹ CNTs with different wall numbers exhibit different individual tube characteristics and film morphology. This study used single-wall carbon nanotubes (SWNTs), multiwall carbon nanotubes (MWNTs), and thin-wall carbon nanotubes (TWNTs) to fabricate conductive and transparent composite films deposited on quartz slide glass. Conductive atomic force microscopy (cAFM) experiments, which are rather new in this still emerging field,³² were conducted to investigate the electrical conductivity of the multilayered CNT composite films. This technique can simultaneously map the topography and current distribution of the multilayered CNT films.³³

Experimental Section

Materials. SWNTs (HiPCO, 35 wt % ash content, CNI Lot no.:P0184) were purchased from Carbon Nanotechnologies, Inc. (Houston, TX). A mild thermal oxidation at 300 °C for one hour was carried out under air to remove amorphous carbon materials. MWNTs and TWNTs used in this study were supplied by Korea University. MWNTs were produced by catalytic chemical vapor deposition (CVD) using Fe–Mo/Al₂O₃ as a

* To whom correspondence should be addressed. E-mail: lhj0630@kist.re.kr. Phone: +82-2-958-5359. Fax: +82-2-958-5309.

[†] Present Address: Max-Planck-Institute for Solid State Research.

[‡] These authors are equally contributed to this paper.

[§] Korea Institute of Science and Technology.

^{||} Yonsei University.

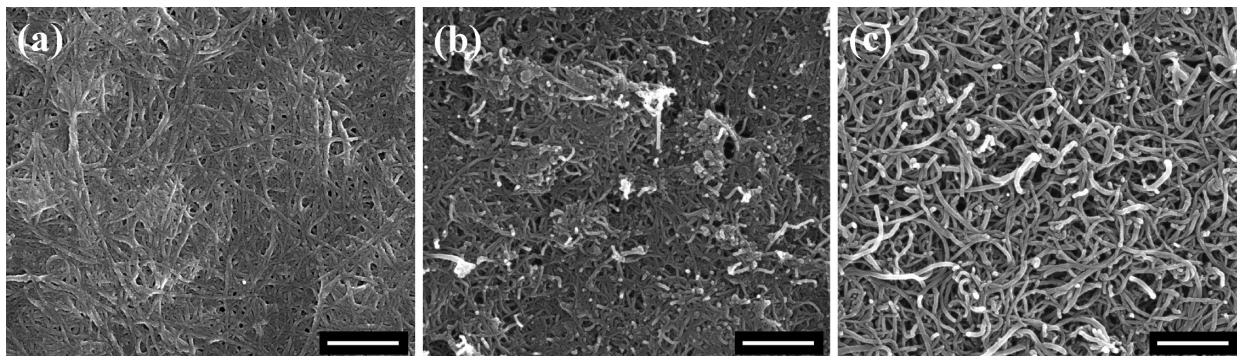


Figure 1. SEM images of bucky papers: (a) SWNT, (b) TWNT, and (c) MWNT. The scale bars in the images indicate 500 nm.

catalyst and C_2H_4 as a carbon source. The diameters of the tubes were 20–30 nm, and the ash content was below 5 wt %. TWNTs were synthesized by catalytic CVD using Fe–Mo/MgO as a catalyst and CH_4 as a carbon source at 900 °C, and their diameters were 5–10 nm. Both MWNTs and TWNTs were treated in a mixture of concentrated sulfuric and nitric acid (95% H_2SO_4 /65% HNO_3 = 3/1, v/v) for one hour to avoid the formation of microsized clusters in the solution.³⁰ Typical transmission electron microscopy (TEM) images for SWNTs, TWNTs, and MWNTs are shown in Figure S1 of the Supporting Information. Poly(vinylalcohol) (PVA; average $M_w \sim 110\,000$) and poly(sodium 4-styrene sulfonate) (PSS; average $M_w \sim 70\,000$) were purchased from Sigma-Aldrich Co.

Preparation of CNT Bucky Papers. To fabricate a bucky paper, 10 mg of CNT in 50 mL of dimethylformamide (DMF) was dispersed through bath ultrasonication, and then, the solution was filtered through a porous 0.2 μm polytetrafluoroethylene (PTFE) filtration membrane. To remove the residual solvent, the CNT film on the membrane was dried at 150 °C for 24 h. To prepare a CNT–PSS composite paper, the same procedure was used with CNT (10 mg) dispersed in 50 mL of a PSS/water (1 wt %) solution.

Preparation of Dispersed-CNT Solution. PSS (0.5 g) was dissolved in 50 mL of deionized (DI) water. CNTs (10 mg) were dispersed in the PSS solution through 3 h of mild sonication in an ultrasonic bath (Elma Transsonic TI-H-5). The dispersions with 0.2 mg/mL CNTs were centrifuged at 5000 rpm, and then, the supernatant was collected, which became one component of the LBL fabrication (PSS–CNT solution; PSS–SWNT, PSS–MWNT, and PSS–TWNT).

Preparation of LBL Film. LBL films were constructed on quartz slide glass. Before deposition, the substrates were cleaned with a mixture of H_2O_2 and concentrated sulfuric acid (3/7, v/v) at room temperature for one hour, rinsed several times with water, and dried with nitrogen gas. After the cleaning process, the substrate was activated to introduce a negative charge on the surface of the substrate by means of a standard treatment solution known as “RCA” (because it was developed by Radio Corporation of America), which was a mixture of ammonium hydroxide (NH_4OH), hydrogen peroxide (H_2O_2), and DI water (H_2O).³⁴ Briefly, the quartz slides were immersed in a solution containing 5 parts H_2O , 1 part NH_4OH , and 1 part H_2O_2 , heated to 70 °C for 30 min, and afterward thoroughly rinsed with DI water. A PVA solution (1 wt %, aqueous) was prepared for use in place of a positively charged component. Clean substrates were immersed in the PVA solution for 20 min followed by rinsing in water three times (each for one min) and drying with nitrogen gas. Then, the substrates were immersed in the oppositely charged PSS solution (1 wt %, aqueous) for 20 min and subjected to the same rinsing procedure. This process was

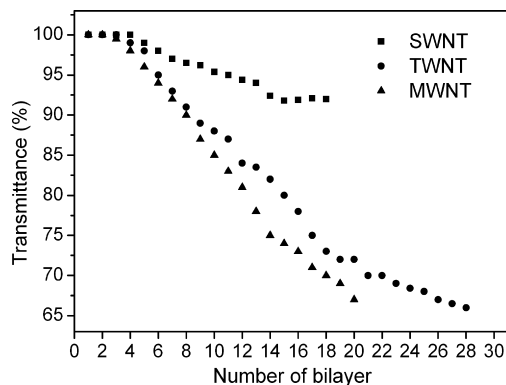


Figure 2. Dependence of the transmittance of the $[PVA/CNT-PSS]_n$ film on the number of bilayers.

repeated twice more to prepare the substrate to be homogeneously coated with polyelectrolyte. All substrates used in this LBL film construction have three bilayers; the bottom layer essentially consisted of PVA and PSS. After the third deposition, the layer of PSS was replaced with a layer of PSS–CNT followed by rinsing in DI water three times and drying with nitrogen gas. To denote LBL assemblies, $[(PVA/PSS)_3(PVA/PSS-CNT)]_n$ was used, in which n represents the number of repeated dipping processes in PVA and PSS–CNT solutions.

Instrumental Analysis. Ultraviolet–visible–near infrared (UV–vis–NIR) optical absorbance spectra analysis and transmission measurement were carried out on a Jasco V-570 spectrophotometer. Electrical conductivity measurements of multilayered films on the glass substrate were performed using a four-probe method. The probe head used was a 4-point cylindrical probe head (JANDEL Engineering Ltd.). A direct current (DC) precision power source (Keithley, Model 6220) and nanovoltmeter (Keithley, Model 2182A) were used for all measurements. Scanning electron microscopy (SEM) images were obtained using a Nova NanoSEM 600 (FEI Co.). Atomic force microscopy (AFM) images of the LBL thin films were recorded under room temperature in a commercial AFM (Asylum Research MFP3D) in noncontact mode (alternating current (AC) mode) with 10 nm standard cantilevers (AC160TS, Olympus). cAFM imaging was performed using the ORCA module (Asylum Research MFP-3D) in noncontact mode with a doped Si tip, Electri-Lever (AC240TM, Olympus). The sample bias was applied to the silver electrode coated on the multilayered film via a wire from the ORCA holder.

Results and Discussion

This study adopted an LBL self-assembly method to prepare a transparent conductive composite film. Three types of tubes

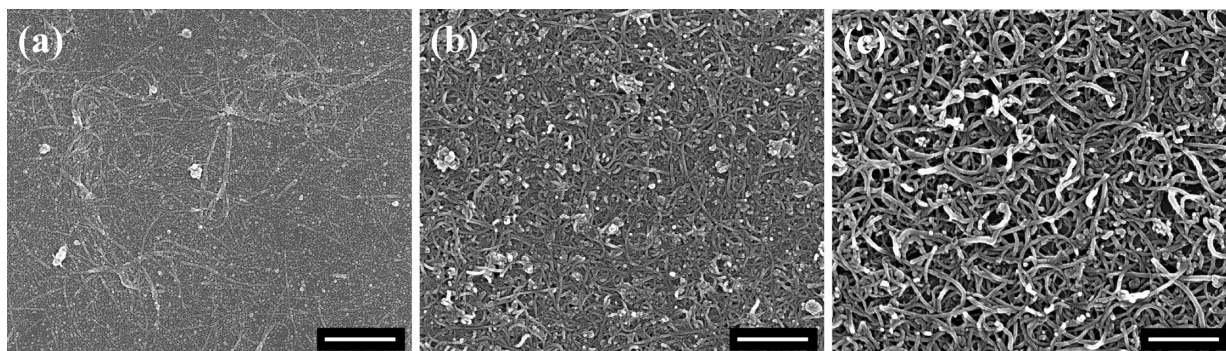


Figure 3. SEM morphology of multilayered film on the Si wafer after thermal annealing at 300 °C for one hour: (a) [(PVA/PSS)₃(PVA/SWNT-PSS)₁₅], (b) [(PVA/PSS)₃(PVA/TWNT-PSS)₂₅], and (c) [(PVA/PSS)₃(PVA/MWNT-PSS)₁₇]. The scale bars in the images indicate 500 nm.

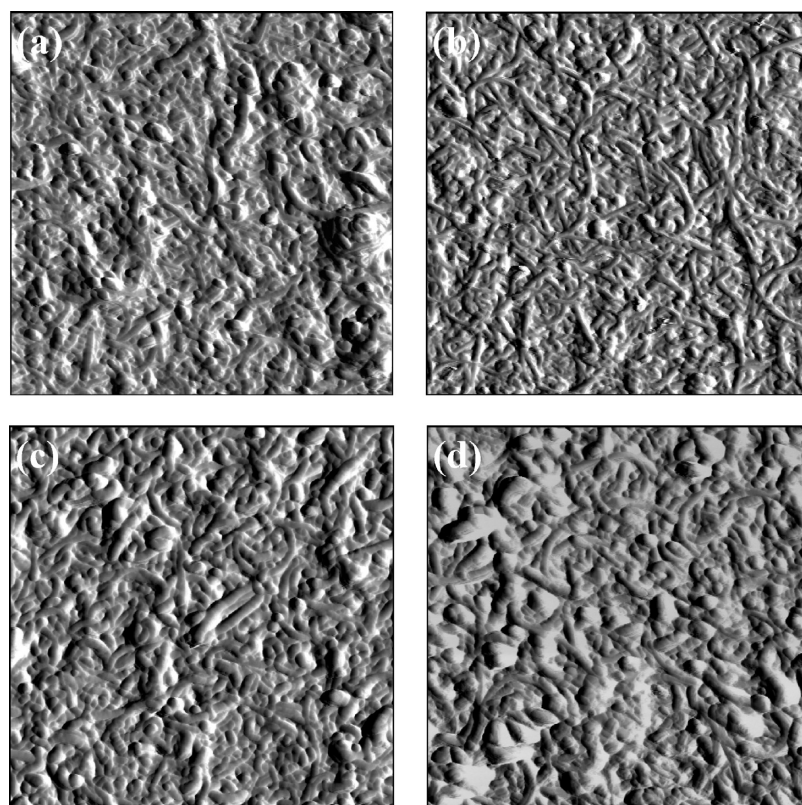


Figure 4. AFM images (amplitude mode): (a) [(PVA/PSS)₃(PVA/(TWNT-PSS))₂₅] and (b) [(PVA/PSS)₃(PVA/(TWNT-PSS))₂₅] after thermal annealing; (c) [(PVA/PSS)₃(PVA/(MWNT-PSS))₁₇] and (d) [(PVA/PSS)₃(PVA/(MWNT-PSS))₁₇] after thermal annealing. The image size is 2 μm × 2 μm.

with different wall numbers were used: SWNTs, TWNTs, and MWNTs. To compare the electrical properties of the as-prepared CNT samples, we fabricated SWNT, TWNT, and MWNT bucky papers using CNT/DMF solution. The film thickness was 6, 6, and 8 μm for SWNTs, TWNTs, and MWNTs, respectively. These films were expected to demonstrate the best electrical conductivity that CNTs can reach without controlling their film transparency. We also prepared composite films using CNT/PSS/water dispersion to examine the effect of PSS on their electrical conductivities before applying the LBL assembly method, in which the PSS solution was used as a dispersing medium for CNTs. The electrical conductivities were measured using a four-point method on five different positions for each sample. Figure 1(a)–(c) presents the SEM images of each bucky paper consisting of different CNTs. In Figure 1(a), SWNTs and TWNTs form a densely packed network (apparent density of SWNT and TWNT bucky papers: 1.3–1.5 g/cm³), whereas MWNT bucky papers form a loosely entangled network

(apparent density of MWNT bucky paper: 0.8–1.0 g/cm³). CNTs with higher wall numbers appear to be curved and flexible, producing a much rougher surface that embeds more air voids in bucky papers. The surface resistance of SWNT, TWNT, and MWNT bucky papers was 2.7, 37, and 19 Ω/sq, respectively (See the Supporting Information for photographs of each bucky paper). When the PSS polymer was incorporated into the CNT solution, the surface resistances of the CNT-PSS composite films clearly changed. The SWNT-PSS composite film showed the highest surface resistance (1200 Ω/sq), and those of the TWNT-PSS and MWNT-PSS composite films were 120 and 20 Ω/sq, respectively. The surface resistance of SWNT-PSS and TWNT-PSS composite films increased greatly compared to those of CNT bucky papers due to the insulating influence of PSS. MWNT films showed very similar values with or without PSS, which can be understood by taking into account the characteristics of electrical resistance in CNT films. The electrical resistance (R_{film}) is associated with the

TABLE 1: Characteristics of Multilayered Composite Films Using TWNT and MWNT

film	thickness (nm)	average thickness increments of each bilayer (nm) ^a	roughness _{rms} (nm)
[(PVA/PSS) ₃ (PVA/(TWNT-PSS))] ₂₅	191	7.6	14.8
[(PVA/PSS) ₃ (PVA/(TWNT-PSS))] ₂₅ after thermal annealing	76	3.0	12.6
[(PVA/PSS) ₃ (PVA/(MWNT-PSS))] ₁₇	233	14	18.4
[(PVA/PSS) ₃ (PVA/(MWNT-PSS))] ₁₇ after thermal annealing	150	8.8	19.3

^a Calculated by the total number of bilayers and film thickness, ignoring the thickness of the initial three layers.

intrinsic resistance of CNTs (R_{CNTs}) and the CNT–CNT contact resistance (R_{contact}) between nanotubes.³⁵ Most SWNTs are semiconducting, and some metallic SWNTs in bundled form gain conductive channels with a small energy gap or pseudogap of approximately 0.1 eV due to intertube interaction in the bundle.^{36,37} In SWNT bucky paper films showing densely packed networks, there are many contact points, which cause conductive channels to open readily. TWNTs cannot open conductive channels as easily, and TWNT bucky paper films show higher resistance than SWNT films, even though they had densely packed networks. The existence of an insulating layer, such as a polymer, makes the opening of conductive channels difficult since the number of contacts decreases, leading to an increase in CNT–CNT contact resistance (R_{contact}) ($R_{\text{contact}} \gg R_{\text{CNTs}}$) in SWNT and TWNT bucky papers. In the case of MWNT films, it is known that the large diameter of the outermost shell causes the gap to reach 0 eV and MWNTs possess more conductive π channels and demonstrate higher conductance than SWNTs or TWNTs.³⁸ However, in a loosely packed network in MWNT bucky paper film, many air voids already exist as an insulating layer; these were later replaced by polymer layers, which did not cause a large change in conductivity, even in the presence of PSS.

The filtration method to fabricate bucky papers was not suitable to control the film transmittance for TCFs. Therefore, the LBL assembly method was used to control the film thickness in order to reach desirable transmittance and to disperse CNTs into the polymer homogeneously.^{27,39,40} PSS was chosen as a negatively charged polyelectrolyte, and PVA was chosen in place of a positively charged component due to its specific affinity to nanotubes, as used for high-strength materials.^{41–43} These polymers were expected to wrap nanotubes in multilayered film, producing the homogeneity of nanotube distribution on the substrate.

We monitored the process of LBL assembly using the UV–vis spectra. The absorbance increased linearly as each bilayer of [PVA/(CNT–PSS)]_n was deposited (see the Supporting Information). At this point, it is worthwhile to notice that the absorbance values were measured using the CNT deposited film on both sides of glass substrates. In order to find the relationship between transmittance and surface resistance for each film, we replaced the measured absorbance into transmittance values for one-sided coated film, which are displayed in Figure 2. Figure 2 shows the linear behavior of film transmittance as a function of n , the number of bilayers deposited on both sides of a quartz slide. An initial lag period in the accumulation of LBL multilayers indicated that the initial three bilayers of (PVA/PSS)₃ were buffer layers on the substrate. The process of LBL assembly continued until the transmittance of the deposited film on one side of the quartz slide reached approximately 65%. Comparing the values of transmittance at the same number of bilayers, it was found that more nanotubes were deposited on the substrates with increasing wall numbers (MWNTs > TWNTs \gg SWNTs). In the case of SWNTs, there

TABLE 2: Surface Resistance at Each Transmittance for Three Different Types of CNTs^a

transmittance (%)	SWNT	TWNT	MWNT
92	6500 k Ω /sq (2400 k Ω /sq)	-	-
87	-	170 k Ω /sq	>1800 k Ω /sq
78	-	99 k Ω /sq	170 k Ω /sq
70	-	54 k Ω /sq (6.4 k Ω /sq)	320 k Ω /sq (8.0 k Ω /sq)

^a The value in the blanket indicates the surface resistance after thermal annealing.

were technical difficulties in fabricating the uniform multilayered film of [(PVA/PSS)₃(PVA/SWNT–PSS)]_n with lower transmittance (less than 90%; i.e., $n = 15$) because of stickiness or charge neutralization on the film surface. The relatively higher loading amount of polymers at each deposition disturbed the successive deposition of SWNTs.

To create closer contacts between individual nanotubes in the network, the multilayered films were treated by thermal annealing at 300 °C for one hour in air. Figure 3 shows the SEM images for the thermally treated films with similar transparency (ca. 65%). However, the SWNT-based composite film in Figure 3(a) had 95% transmittance and showed very weak networking and high resistance due to the low content of nanotubes; this was excluded in further discussion. In Figure 3(b, c), TWNTs and MWNTs formed randomly connected networks in the multilayered composite film, which appear to be as dense as those of the bucky papers in Figure 1. TWNTs had more straight shapes, of which a multilayered film showed a densely packed network. MWNTs had a more curved shape, and there were large amounts of free space between nanotubes, forming a loosely packed network. Even after thermal annealing, the overall morphologies did not change, and they were not distinguished by SEM. However, AFM analysis clearly revealed the changes in the surface morphologies of the thin composite films. The morphologies of each film surface before and after thermal annealing are shown in Figure 4. We compared the differences in the film morphology before annealing (Figure 4(a, b)) and after annealing (Figure 4(c, d)). Table 1 summarizes the composite film thickness, average thickness increment of each bilayer, and surface roughness, as measured by AFM. By assuming that the same transmittance corresponds to the same amount of nanotubes on the substrate, a larger film thickness and rougher surface indicated that the MWNT–polymer composite film had a much more porous structure than the other films. After thermal annealing, the MWNT–polymer composite film remained porous, but it was much rougher due to the curved and entangled network structure of MWNTs, whereas the thickness of TWNT–polymer composite film decreased by more than half and the roughness also showed a small decrease, which indicates the formation of a much more compact structure. The diameters of TWNT and MWNT were measured as approximately 7 and 20 nm, respectively, from TEM analysis (see

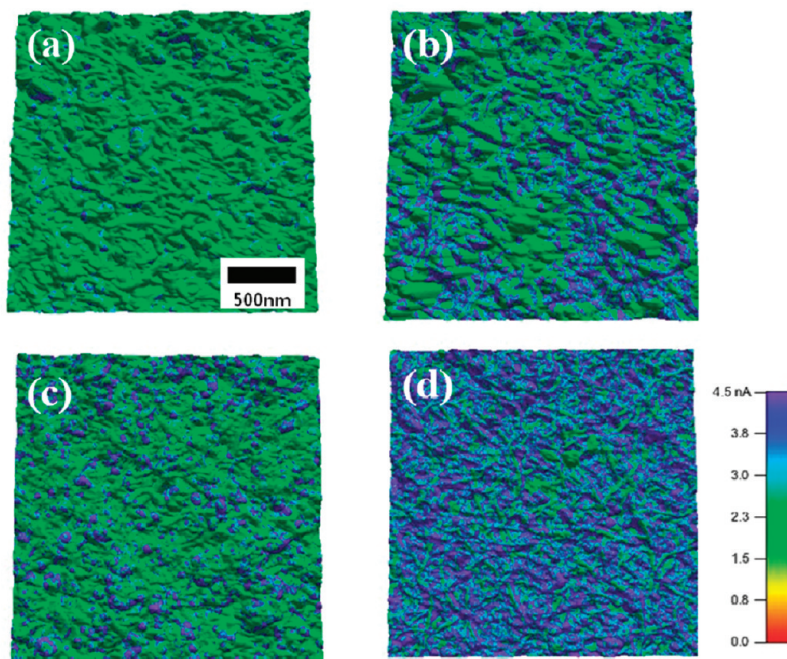


Figure 5. Current channel overlays on the topography of the multilayered films (a, c) before annealing (bias = 1 V) and (b, d) after annealing (bias = 150 mV); (a, b) [(PVA/PSS)₃(PVA/MWNT-PSS)₁₇] and (c, d) [(PVA/PSS)₃(PVA/TWNT-PSS)₂₅]. The image size is 2 μm \times 2 μm .

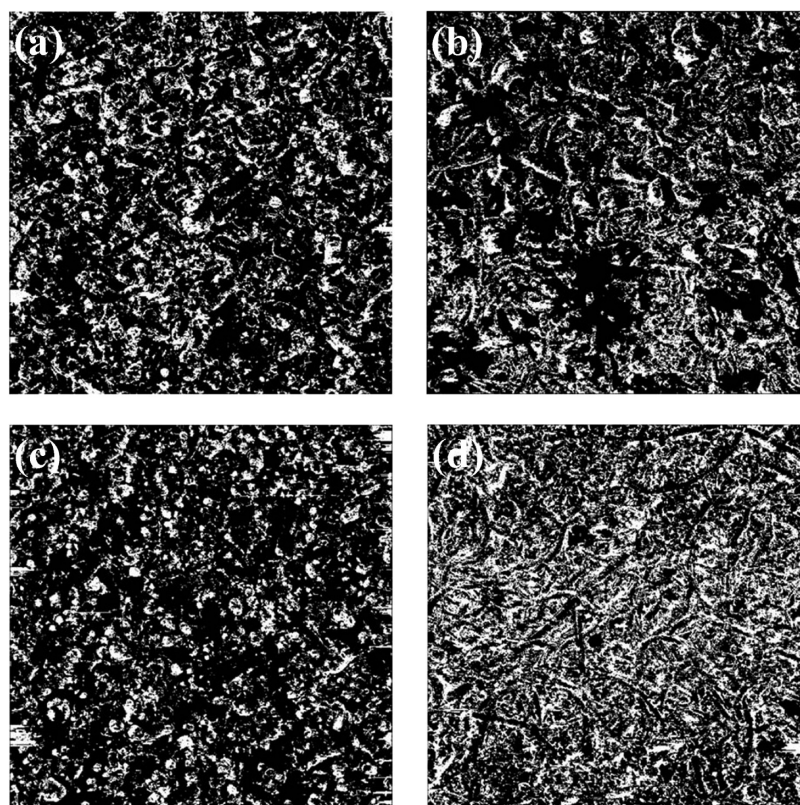


Figure 6. Black-and-white images converted from the images in Figure 5: (a, c) before annealing (bias = 1 V) and (b, d) after annealing (bias = 150 mV); (a, b) [(PVA/PSS)₃(PVA/MWNT-PSS)₁₇] and (c, d) [(PVA/PSS)₃(PVA/TWNT-PSS)₂₅]. The image size is 2 μm \times 2 μm .

the Supporting Information). This corresponds well with the average thickness increment of 7.6 and 14 nm, respectively, calculated from AFM measurement (see the Supporting Information for photographs of the multilayered films deposited on glass).

This study compared the electrical conductivities of thin multilayered composite films having different types of CNTs. The surface resistance of the SWNT-polymer composite film

was much higher (about 6500 Ω/sq) than those of TWNT or MWNT films at a similar transparency, which implies that PSS interacts with SWNTs and plays a role as an insulating matrix. It was already mentioned that a significant increase in resistance was found in SWNT-PSS bucky papers prepared using a simple filtration method. The SWNT-polymer composite film showed scattered values in transmittance and surface resistance due to the heterogeneous surface, so these values were not included

in Table 1. Table 2 shows the surface resistances of [(PVA/PSS)₃(PVA/TWNT-PSS)_n] and [(PVA/PSS)₃(PVA/MWNT-PSS)_n] depending on the transmittance at 550 nm. The results show that the resistance of the thin composite film with TWNTs decreases more rapidly than that with MWNTs; it showed the lowest value of 70% transmittance at 550 nm. In recent reports,^{44,45} double-wall nanotubes (DWNTs) are desirable for use as transparent conductive materials, considering both transparency and electrical conductivity, since SWNTs usually contain semimetallic characteristics and MWNTs have strong optical absorption. It seems to coincide with the present result by expanding up to TWNTs.

We investigated the conductive behavior of CNT-polymer multilayered composite films depending on the type of CNTs by incorporating cAFM. cAFM produces useful information about the morphology and current map of composite films, which explains how current paths are constructed in multilayered composite films. Neither the [(PVA/PSS)₃(PVA/TWNT-PSS)₂₅] nor the [(PVA/PSS)₃(PVA/MWNT-PSS)₁₇] multilayered films, which have a transmittance of 70% before annealing, show clear paths of electrical current on the films (Figure 5 (a, c)), even though a 1 V bias was applied. However, after annealing the films at 300 °C for one hour, each current path of the films was shown more clearly (Figure 5 (b, d)) with even lower bias (150 mV). In addition, the [(PVA/PSS)₃(PVA/TWNT-PSS)₂₅] multilayered film shows more homogeneous current distribution over the samples than the [(PVA/PSS)₃(PVA/MWNT-PSS)₁₇] film. To evaluate the quantitative comparison of conductive channel distribution, we modified the cAFM images in Figure 5 to black and white using the image analysis program Image-J (Figure 6). A specific current value was set as a threshold value, and the pixels over a threshold value were displayed in white. The white areas (i.e., conductive channels) were calculated as 12 and 10% for MWNT- and TWNT-based composite films, respectively. This value increased up to 29% in a TWNT-polymer composite film after thermal annealing, which is two times larger than that of MWNT-polymer composite film (13%). This study supports that TWNT with a diameter less than 10 nm would be a desirable CNT material, especially for CNT-polymer composite films as TCFs. The surface resistance of [(PVA/PSS)₃(PVA/TWNT-PSS)₂₅] multilayered film is still high for real applications, even though the dispersion of TWNTs in the polymer was well-controlled. Therefore, a hybrid type of filler would be required to achieve the ideal goal of TCFs.

Conclusion

This study compared three different types of CNTs for use as conductive fillers in thin multilayered composite films for TCFs. The LBL assembly method was used to control the dispersion of CNTs within polymer materials as well as the transmittance of the CNT-polymer composite film. In addition, the electrical conductivity of CNT-polymer multilayered films was visualized and qualitatively and quantitatively compared using cAFM. Under the controlled system, the TWNT shows the most desirable properties among CNT materials for use as conductive fillers, especially for CNT-polymer composite films for TCFs. TWNTs showed closer packing morphology than MWNTs and better conductivity, even with a polymer, than SWNTs. However, the electrical conductivity of TWNT-polymer multilayered film was still not high enough for use in TCFs. The electrical conductivity enhancement in CNT-based transparent conductive composite films is of interest for their performance in optoelectronic devices and electrochromic and electrochemical light-emitting and solar cells.

Acknowledgment. This study was supported in part by research grants from the Ministry of Commerce, Industry, and Energy through the Materials and Component Technology Development Program in the Republic of Korea. The authors are grateful for the supply of TWNTs and MWNTs from Professor Cheol Jin Lee at Korea University.

Supporting Information Available: Typical transmission electron microscopy (TEM) images for SWNTs, TWNTs, and MWNTs are shown in Figure S1. TEM images were taken on a field emission gun transmission electron microscope (Technai G2). Figure S2 shows the photographs of each bucky paper prepared for SWNTs, TWNTs, and MWNTs corresponding to the SEM images in Figure 1. Figure S3 shows an increase of the absorbance as each bilayer of [PVA/(CNT-PSS)]_n was deposited during the process of LBL assembly. Transmittance values at 550 nm in Figure S3 were used in displaying the linear behavior of film transmittance as a function of *n*, the number of bilayers in Figure 2. This material is available free of charge via the Internet at <http://pubs.acs.org>.

References and Notes

- (1) Groning, P.; Ruffieux, P.; Schlapbach, L.; Groning, O. *Adv. Eng. Mater.* **2003**, *5*, 541.
- (2) Noda, K.; Sato, H.; Itaya, H.; Yamada, M. *Jpn. J. Appl. Phys. Part 1-Regul. Pap. Short Notes Rev. Pap.* **2003**, *42*, 217.
- (3) Brabec, C. J.; Sariciftci, N. S.; Hummelen, J. C. *Adv. Funct. Mater.* **2001**, *11*, 15.
- (4) Jung, K. H.; Hong, J. S.; Vittal, R.; Kim, K. J. *Chem. Lett.* **2002**, 864.
- (5) Jang, S. R.; Vittal, R.; Kim, K. J. *Langmuir* **2004**, *20*, 9807.
- (6) Gu, G.; Burrows, P. E.; Venkatesh, S.; Forrest, S. R.; Thompson, M. E. *Opt. Lett.* **1997**, *22*, 172.
- (7) Zhang, D.; Ryu, K.; Liu, X.; Polikarpov, E.; Ly, J.; Tompson, M. E.; Zhou, C. *Nano Lett.* **2006**, *6*, 1880.
- (8) Saran, N.; Parikh, K.; Suh, D. S.; Munoz, E.; Kolla, H.; Manohar, S. K. *J. Am. Chem. Soc.* **2004**, *126*, 4462.
- (9) Song, Y. I.; Yang, C.-M.; Kim, D. Y.; Kanoh, H.; Kaneko, K. *J. Colloid Interface Sci.* **2008**, *318*, 365.
- (10) Zhang, M.; Fang, S. L.; Zakhidov, A. A.; Lee, S. B.; Aliev, A. E.; Williams, C. D.; Atkinson, K. R.; Baughman, R. H. *Science* **2005**, *309*, 1215.
- (11) Ferrer-Anglada, N.; Kaempgen, M.; Skakalova, V.; Dettlaff-Weglikowska, U.; Roth, S. *Diam. Relat. Mat.* **2004**, *13*, 256.
- (12) Kong, B. S.; Jung, D. H.; Oh, S. K.; Han, C. S.; Jung, H. T. *J. Phys. Chem. C* **2007**, *111*, 8377.
- (13) Bocharova, V.; Kiriy, A.; Oertel, U.; Stamm, M.; Stoffelbach, F.; Jerome, R.; Detrembleur, C. *J. Phys. Chem. B* **2006**, *110*, 14640.
- (14) Cao, Q.; Rogers, J. A. *Adv. Mater.* **2009**, *21*, 29.
- (15) Hu, L.; Hecht, D. S.; Gruner, G. *Nano Lett.* **2004**, *4*, 2513.
- (16) Geng, H.-Z.; Kim, K. K.; So, K. P.; Lee, Y. S.; Chang, Y.; Lee, Y. H. *J. Am. Chem. Soc.* **2007**, *129*, 7758.
- (17) Ericson, L. M.; Hauge, R. H.; Smalley, R. E. *Chem. Mater.* **2002**, *15*, 175.
- (18) Meitl, M. A.; Zhou, Y. X.; Gaur, A.; Jeon, S.; Usrey, M. L.; Strano, M. S.; Rogers, J. A. *Nano Lett.* **2004**, *4*, 1643.
- (19) Armitage, N. P.; Gabriel, J. C. P.; Gruner, G. *J. Appl. Phys.* **2004**, *95*, 3228.
- (20) De, S.; Lyons, P. E.; Sorel, S.; Doherty, E. M.; King, P. J.; Blau, W. J.; Nirmalraj, P. N.; Boland, J. J.; Scardaci, V.; Joimel, J.; Coleman, J. N. *ACS Nano* **2009**, *3*, 714.
- (21) Ham, H. T.; Choi, Y. S.; Chee, M. G.; Cha, M. H.; Chung, I. J. *Polym. Eng. Sci.* **2008**, *48*, 1.
- (22) Bauhofer, W.; Kovacs, J. Z. *Compos. Sci. Technol.* **2008**, in press.
- (23) Blighe, F. M.; Hernandez, Y. R.; Blau, W. J.; Coleman, J. N. *Adv. Mater.* **2007**, *19*, 4443.
- (24) Decher, G.; Schlenoff, J. B. *Multilayer Thin Films: Sequential Assembly of Nanocomposite Materials*; Wiley-VCH Verlag GmbH & Co.: Weinheim, Germany, 2003.
- (25) Mamedov, A. A.; Kotov, N. A.; Prato, M.; Guldi, D. M.; Wicksted, J. P.; Hirsch, A. *Nat. Mater.* **2002**, *1*, 190.
- (26) Rouse, J. H.; Lillehei, P. T. *Nano Lett.* **2003**, *3*, 59.
- (27) Shim, B. S.; Tang, Z.; Morabito, M. P.; Agarwal, A.; Hong, H.; Kotov, N. A. *Chem. Mater.* **2007**, *19*, 5467.
- (28) Park, H. J.; Kim, J.; Chang, J. Y.; Theato, P. *Langmuir* **2008**, *24*, 10467.

- (29) Zhongrui, L.; Hom, R. K.; Enkeleda, D.; Viney, S.; Alexandru, S. B.; Alexandru, R. B.; Dan, L. *Appl. Phys. Lett.* **2007**, *91*, 053115.
- (30) Park, H. J.; Park, M.; Chang, J. Y.; Lee, H. *Nanotechnology* **2008**, *19*.
- (31) Li, Z. R.; Kandel, H. R.; Dervishi, E.; Saini, V.; Xu, Y.; Biris, A. R.; Lupu, D.; Salamo, G. J.; Biris, A. S. *Langmuir* **2008**, *24*, 2655.
- (32) Dai, H.; Wong, E. W.; Lieber, C. M. *Science* **1996**, *272*, 523.
- (33) Rispal, L.; Stefanov, Y.; Wessely, F.; Schwalke, U. *Jpn. J. Appl. Phys. Part 1—Regul. Pap. Brief Commun. Rev. Pap.* **2006**, *45*, 3672.
- (34) Donose, B. C.; Taran, E.; Vakarelski, I. U.; Shinto, H.; Higashitani, K. *J. Colloid Interface Sci.* **2006**, *299*, 233.
- (35) Bae, D. J.; Kim, K. S.; Park, Y. S.; Suh, E. K.; An, K. H.; Moon, J. M.; Lim, S. C.; Park, S. H.; Jeong, Y. H.; Lee, Y. H. *Phys. Rev. B* **2001**, *64*, 233401/1.
- (36) Delaney, P.; Choi, H. J.; Ihm, J.; Louie, S. G.; Cohen, M. L. *Nature* **1998**, *391*, 466.
- (37) Ouyang, M.; Huang, J. L.; Cheung, C. L.; Lieber, C. M. *Science* **2001**, *292*, 702.
- (38) Skakalova, V.; Kaiser, A. B.; Woo, Y.-S.; Roth, S. *Phys. Rev. B* **2006**, *74*, 085403.
- (39) Yan, X. B.; Chen, X. J.; Tay, B. K.; Khor, K. A. *Electrochem. Commun.* **2007**, *9*, 1269.
- (40) Bertoni, C.; Skakalova, V.; Roth, S. *Physica E* **2008**, *40*, 2257.
- (41) Dalton, A. B.; Collins, S.; Munoz, E.; Razal, J. M.; Ebron, V. H.; Ferraris, J. P.; Coleman, J. N.; Kim, B. G.; Baughman, R. H. *Nature* **2003**, *423*, 703.
- (42) Vigolo, B.; Penicaud, A.; Coulon, C.; Sauder, C.; Pailler, R.; Journet, C.; Bernier, P.; Poulin, P. *Science* **2000**, *290*, 1331.
- (43) Zhang, M.; Atkinson, K. R.; Baughman, R. H. *Science* **2004**, *306*, 1358.
- (44) Endo, M.; Hayashi, T.; Muramatsu, H.; Kim, Y. A.; Terrones, H.; Terrones, M.; Dresselhaus, M. S. *Nano Lett.* **2004**, *4*, 1451.
- (45) Ren, W. C.; Li, F.; Chen, J. A.; Bai, S.; Cheng, H. M. *Chem. Phys. Lett.* **2002**, *359*, 196.

JP901684K